10. H. King *et al.*, *Earth Planet. Sci. Lett.* **300**, 11–18 (2010).
11. F. Robert, D. Gautier, B. Dubrulle, *Space Sci. Rev.* **92**, 201–224 (2000).
12. C. M. Alexander *et al.*, *Science* **337**, 721–723 (2012).
13. F. Robert, *Science* **293**, 1056–1058 (2001).
14. L. Hallis, G. Taylor, K. Nagashima, G. Huss, *Earth Planet. Sci. Lett.* **359–360**, 84–92 (2012).
15. Q. Zhou *et al.*, *Geochim. Cosmochim. Acta* **110**, 152–175 (2013).
16. K. Misawa, A. Yamaguchi, K. Hiroshi, *Geochim. Cosmochim. Acta* **69**, 5847–5861 (2005).
17. R. N. Clayton, N. Onuma, T. K. Mayeda, *Earth Planet. Sci. Lett.* **30**, 10–18 (1976).
18. T. B. McCord, J. B. Adams, T. V. Johnson, *Science* **168**, 1445–1447 (1970).
19. H. Y. McSween Jr., D. W. Mittlefehldt, A. W. Beck, R. G. Mayne, T. J. McCoy, in *The Dawn Mission to Minor Planets 4 Vesta and 1 Ceres* (Springer, New York, 2012), pp. 141–174.
20. See supplementary materials on *Science* Online.
21. $\delta D = \{[(D/H_{unknown})/(D/H_{VSMOW})] - 1\} \times 1000$, where VSMOW = Vienna standard mean ocean water.
22. Z. D. Sharp, F. M. McCubbin, C. K. Shearer, *Earth Planet. Sci. Lett.* **380**, 88–97 (2013).
23. R. Tartèse *et al.*, *Geology* **42**, 363–366 (2014).
24. T. Chacko, D. R. Cole, J. Horita, *Rev. Mineral. Geochem.* **43**, 1–81 (2001).
25. Y. Miura, N. Sugiura, *Antarctic Meteor. Res.* **6**, 338 (1993).
26. A. Morbidelli *et al.*, *Meteorit. Planet. Sci.* **35**, 1309–1320 (2000).
27. D. P. O'Brien, K. J. Walsh, A. Morbidelli, S. N. Raymond, A. M. Mandell, *Icarus* **239**, 74–84 (2014).

ACKNOWLEDGMENTS

We thank the anonymous reviewers; K. Righter, D. Ebel, C. Agee, and T. McCoy for sample allocations; and N. Shimizu and G. Gaetani for their immense help. Supported by NASA graduate fellowship NNX13AR90H (A.R.S.), an Andrew W. Mellon Foundation Award for Innovative Research (S.G.N.), and NASA Cosmochemistry Program award NNX11AG76G (F.M.M.). Secondary ion mass spectrometry analyses were made at the Northeast National Ion Microprobe Facility (NENIMF) at the Woods Hole Oceanographic Institution (WHOI). NENIMF acknowledges support from the NSF Instrumentation and Facilities Program, Division of Earth Sciences, and from WHOI. Data are presented in the main text of the manuscript and the supplementary materials.

SUPPLEMENTARY MATERIALS

www.sciencemag.org/content/346/6209/623/suppl/DC1
Materials and Methods
Supplementary Text
Figs. S1 and S2
Table S1
References (*28*–*81*)

30 May 2014; accepted 29 September 2014
10.1126/science.1256717

NEURODEVELOPMENT

Dendrite morphogenesis depends on relative levels of NT-3/TrkC signaling

William Joo,[1,2] Simon Hippenmeyer,[1]* Liqun Luo[1,2]†

Neurotrophins regulate diverse aspects of neuronal development and plasticity, but their precise in vivo functions during neural circuit assembly in the central brain remain unclear. We show that the neurotrophin receptor tropomyosin-related kinase C (TrkC) is required for dendritic growth and branching of mouse cerebellar Purkinje cells. Sparse TrkC knockout reduced dendrite complexity, but global Purkinje cell knockout had no effect. Removal of the TrkC ligand neurotrophin-3 (NT-3) from cerebellar granule cells, which provide major afferent input to developing Purkinje cell dendrites, rescued the dendrite defects caused by sparse TrkC disruption in Purkinje cells. Our data demonstrate that NT-3 from presynaptic neurons (granule cells) is required for TrkC-dependent competitive dendrite morphogenesis in postsynaptic neurons (Purkinje cells)—a previously unknown mechanism of neural circuit development.

Neurotrophins regulate the survival, differentiation, and plasticity of peripheral and central neurons (*1*–*3*). The mammalian neurotrophin family signals through three tropomyosin-related kinase (Trk) receptors, as well as the p75 neurotrophin receptor (p75NTR). Whereas brain-derived neurotrophic factor (BDNF) has been intensely studied, much less is known about neurotrophin-3 (NT-3) and its receptor, TrkC, despite their widespread expression in the developing and adult brain (*4*, *5*). The lack of central brain cell death in mice lacking NT-3 and TrkC contrasts starkly with the severe reductions in sensory and sympathetic neurons and suggests survival-independent functions (*6*, *7*). NT-3 functions in dendrite morphogenesis in brain slice culture and in proprioceptive axon patterning (*8*–*10*). However, evaluating the roles of NT-3/TrkC signaling in the central brain in vivo has been hindered by the early postnatal lethality of NT-3 or TrkC knockout mice and the limited cellular resolution of phenotypic analyses (*7*, *11*).

To study the cell-autonomous function of TrkC in mouse neural development, we used mosaic analysis with double markers (MADM) (*12*, *13*) with a null allele of *trkC* that removes all isoforms of the receptor (*14*), and a pan-neural *Nestin-Cre* line (*15*) to drive recombination throughout the brain. Thus, in an otherwise heterozygous animal ($trkC^{+/-}$), Cre/*loxP*-mediated mitotic recombination between homologous chromosomes sparsely labels wild-type ($trkC^{+/+}$) and homozygous mutant ($trkC^{-/-}$) cells in distinct colors (figs. S1A and S2). In these animals, sparse $trkC^{-/-}$ cells were labeled with green fluorescent protein (GFP) (green), $trkC^{+/+}$ cells with tdTomato (red), and $trkC^{+/-}$ cells with both GFP and tdTomato (yellow). Cells without recombination, which remained colorless, were all $trkC^{+/-}$. Although survival of central brain cells was not apparently affected by sparse *trkC* removal (figs. S2 and S3A), consistent with previous observations (*6*, *7*), we observed a distinctive Purkinje cell dendrite phenotype (Fig. 1).

Both $trkC^{+/+}$ and $trkC^{+/-}$ Purkinje cells extended complex dendritic arbors that spanned the entire molecular layer of the cerebellum (Fig. 1A, left and middle). In contrast, arbors from $trkC^{-/-}$ cells failed to reach the pial surface (65 out of 72 cells; Fig. 1A, right). These stunted arbors exhibited normal dendritic spine density (fig. S3B), but spanned only ~75% of the molecular layer (Fig. 1B). To determine when the $trkC^{-/-}$ dendrite phenotype emerges, we compared $trkC^{+/+}$ and $trkC^{-/-}$ cells between postnatal day 7 (P7) and P21, when Purkinje cells normally elaborate their dendrites and begin to form synapses (Fig. 1C and fig. S4). Although indistinguishable from control cells at P7 and P10, $trkC^{-/-}$ cells exhibited reduced dendritic arbor height, branch number, and total dendrite length compared to $trkC^{+/+}$ cells by day 14 (Fig. 1, C and D, and fig. S4). Growth and branching phenotypes persisted in 3-month-old animals (Fig. 1, C and D, and fig. S4), indicating that loss of TrkC caused a morphogenesis defect rather than a developmental delay. Furthermore, the most distal dendritic branches were preferentially lost in $trkC^{-/-}$ cells (fig. S3C). Uniparental disomies (*13*) (fig. S5) and fluorescent markers (fig. S6) did not affect Purkinje cell dendrite phenotypes. Thus, our mosaic analysis suggested that TrkC is required cell-autonomously for proper Purkinje cell dendrite growth and branching.

Although Trk signaling normally requires the tyrosine kinase domain (*16*), TrkC also has a kinase-independent role in synaptogenesis (*17*). To determine whether dendritic arborization relies on kinase activity, we examined MADM mice harboring a conditional allele in which *loxP* sites flank an exon encoding part of the TrkC kinase domain (*18*). Here, *Nestin-Cre* mediated interchromosomal recombination within the MADM cassettes, and also excised this exon to generate a "kinase-dead" allele ($trkC^{KD}$; fig. S1B). At P21, Purkinje cells homozygous for this allele ($trkC^{KD/KD}$) exhibited dendrite height, branch number, and total dendritic length phenotypes

[1]Howard Hughes Medical Institute and Department of Biology, Stanford University, Stanford, CA 94305, USA. [2]Neurosciences Program, Stanford University, Stanford, CA 94305, USA.
*Present address: Institute of Science and Technology Austria, 3400 Klosterneuburg, Austria. †Corresponding author. E-mail: lluo@stanford.edu

comparable to those of *trkC*$^{-/-}$ cells (Fig. 2). Thus, proper dendritic arborization requires TrkC kinase activity.

Because perturbing TrkC in a sparse population (0.5 to 1%) of Purkinje cells disrupted their dendritic arbors, we examined how TrkC ablation from all Purkinje cells affects dendrite morphology. Calbindin immunostaining labels Purkinje cells and their dendrites, which normally span the entire molecular layer of the cerebellum (Fig. 3A). *trkC* conditional knockout using Purkinje cell–specific *pcp2-Cre* (*19*) (fig. S1C) did not reduce Purkinje cell dendrite height compared to controls (Fig. 3, A and B). To analyze dendrite branching in more detail, we used MADM cassettes to sparsely label Purkinje cells in the Purkinje cell–specific *trkC* conditional knockout background. In this context, *pcp2-Cre* removed *trkC* from all Purkinje cells, but GFP and tdTomato were reconstituted only in a sparse subset (5 to 10%) of Purkinje cells through interchromosomal recombination

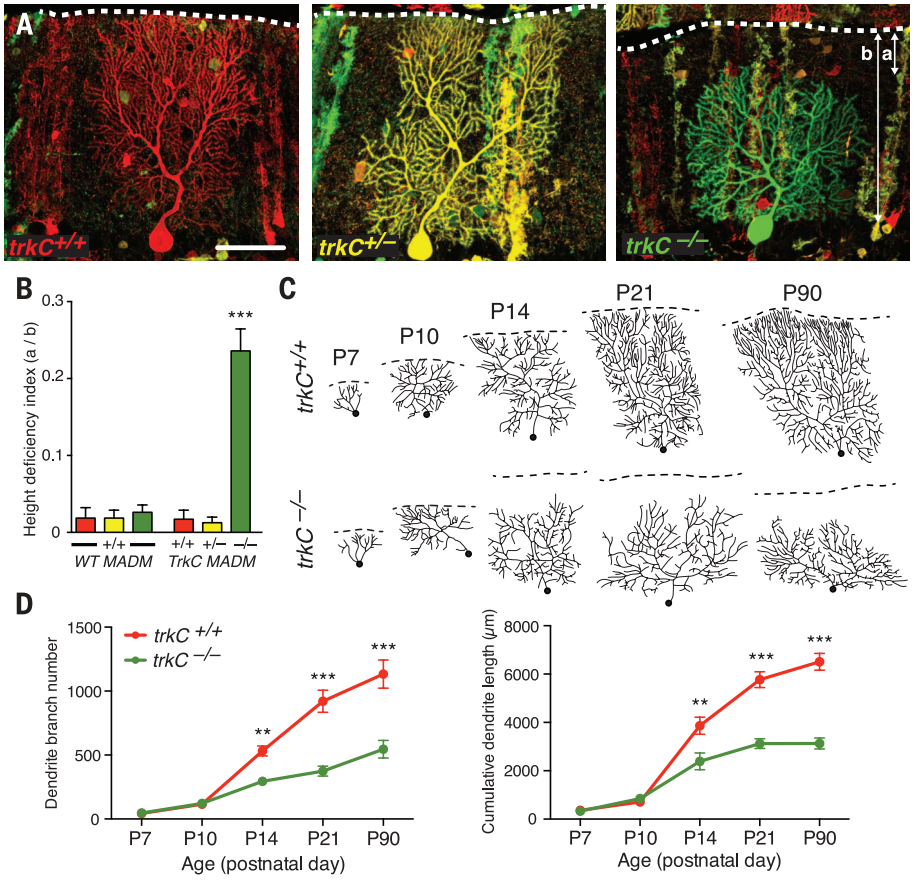

Fig. 1. TrkC is cell-autonomously required for Purkine cell dendritic arborization. (**A**) Postnatal day 21 (P21) red *trkC*$^{+/+}$ and yellow *trkC*$^{+/-}$ Purkinje cell dendritic arbors span the entire molecular layer of the cerebellar cortex. In contrast, *trkC*$^{-/-}$ Purkinje cell dendritic arbors are shorter and fail to reach the pial surface (dashed white lines). Short (a) and long (b) arrows indicate distance from pial surface to top of arbor and molecular layer span, respectively. Scale bar, 50 μm. (**B**) Quantifications of height deficiency index (*a*/*b*) for *WT MADM* and *trkC MADM*. Here and in subsequent figures, all values are means ± SEM. *** $P < 0.001$, one-way analysis of variance (ANOVA) with Tukey's multiple comparisons test. (**C**) Traces of Purkinje cell dendritic arbors between P7 and P90. Dashed lines indicate the external granule layer margin in P7–P10, or the pial surface in P14–90. Dots indicate primary branch start point. (**D**) Quantification of dendrite branch number (left) and cumulative dendrite length (right). Red, *trkC*$^{+/+}$; green, *trkC*$^{-/-}$. ** $P < 0.01$, *** $P < 0.001$, two-way ANOVA with Bonferroni's multiple comparisons test. See table S1 for additional information including *N* for each experiment.

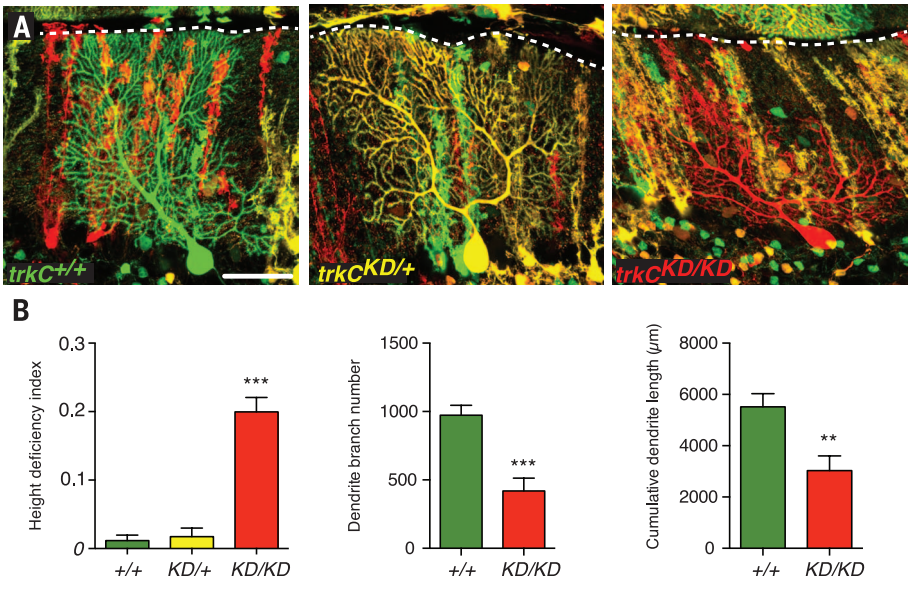

Fig. 2. Dendritic arborization requires TrkC kinase activity. (**A**) Analogous to *trkC*$^{-/-}$ arbors (Fig. 1), *trkC*$^{KD/KD}$ arbors are shorter than those of *trkC*$^{+/+}$ and *trkC*$^{KD/+}$ cells at P21 and fail to reach the pial surface. (**B**) Quantifications of height deficiency index (***$P < 0.001$, one-way ANOVA with Tukey's multiple comparisons test), branch number, and cumulative dendrite length (** $P < 0.01$, *** $P < 0.001$, unpaired *t* test) as in Fig. 1. Also see table S1.

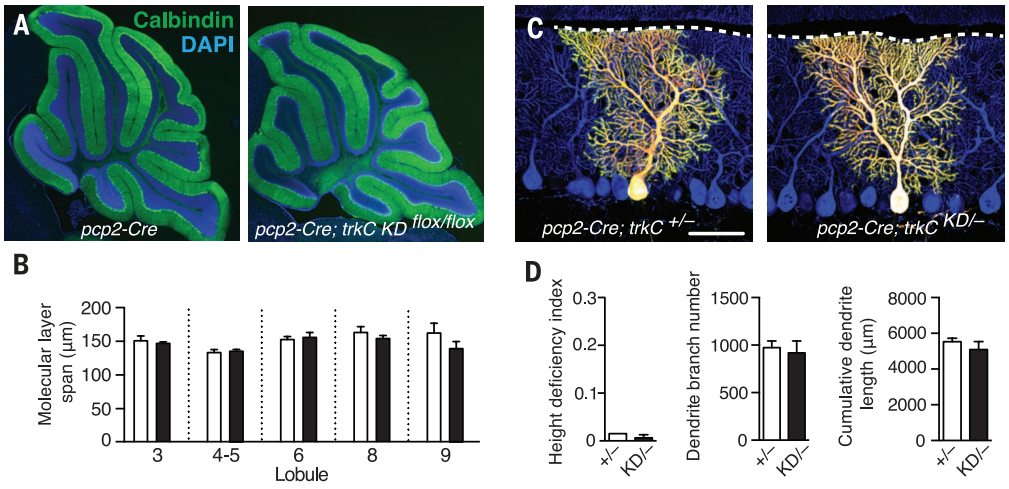

Fig. 3. Normal dendrite morphogenesis when all Purkinje cells lack TrkC. (**A**) Calbindin staining labels Purkinje cells and their dendrites (green). Removing *trkC* from all Purkinje cells (right) does not cause global reductions in dendrite height relative to controls (left) at P21. (**B**) Molecular-layer thickness across multiple lobules was similar for control *pcp2-Cre*$^{+/-}$ (white) and *pcp2-Cre*$^{+/-}$*;trkC KD*$^{flox/flox}$ (black) mice. No significant differences, two-way ANOVA with Tukey's multiple comparisons test. (**C**) *trkC*$^{KD/-}$ Purkinje cells do not exhibit dendrite height or branching defects relative to *trkC*$^{+/-}$ cells. (**D**) Quantifications of height deficiency index, branch number, and cumulative length as in Fig. 1 (no significant differences, unpaired *t* test). Also see table S1. DAPI, 4′,6-diamidino-2-phenylindole

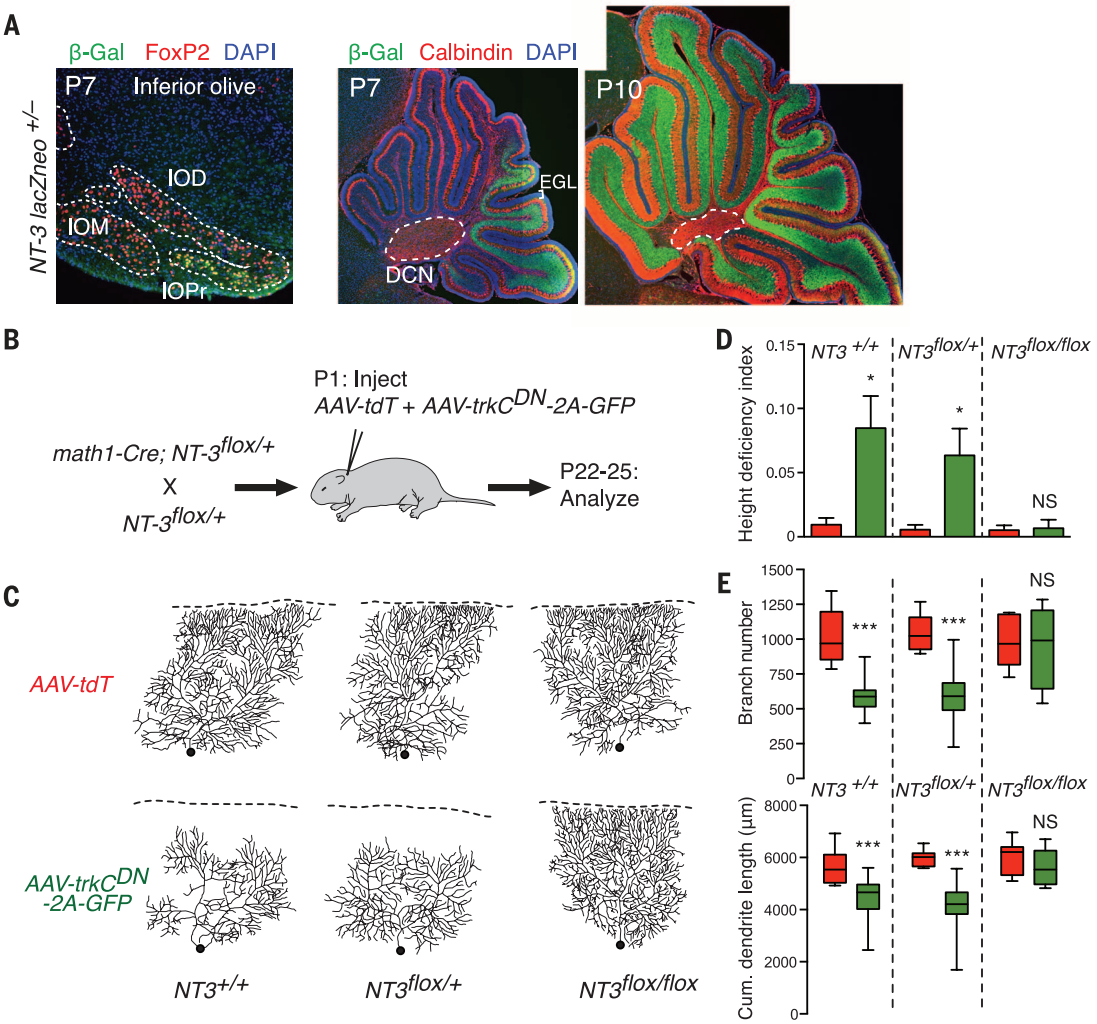

Fig. 4. Testing NT-3/TrkC-dependent competition. (**A**) β-Gal staining reports NT-3 expression patterns in a *NT-3*$^{lacZneo/+}$ knock-in mouse (green). Left: coronal section of the mouse medulla at P7. FoxP2 staining labels inferior olive neurons (red). β-Gal is present in a subset of neurons in the inferior olive principal nucleus (IOPr), but not in the medial or dorsal nuclei (IOM, IOD). Middle and right: At P7, β-Gal is enriched in granule cells of posterior folia. By P10, β-Gal is present in all folia. No signal was detectable in the external granular layer (EGL, bracket), which contains granule cell progenitors. Likewise, no signal was detectable in Purkinje cells or the deep cerebellar nuclei (DCN, dashed line), the postsynaptic targets of Purkinje cells. (**B**) Schematic of a viral approach to test relative NT-3/TrkC signaling in dendrite morphogenesis. Viruses encoding either tdTomato (*AAV-tdT*) or a dominant-negative TrkC together with GFP (*AAV-trkC*^{DN}*-2A-GFP*) were coinjected into *math1-Cre;NT-3*$^{flox/flox}$, *math1-Cre;NT-3*$^{flox/+}$, or control *math1-Cre* mice at P1. tdT or GFP/TrkC^{DN}-expressing Purkinje cells were analyzed 21 to 24 days after injection. (**C**) Dendritic arbors of tdT or GFP/TrkC^{DN}-expressing Purkinje cells. In *math1-Cre;NT-3*$^{+/+}$ or *math1-Cre;NT-3*$^{flox/+}$ mice, TrkC^{DN}-expressing cells exhibited decreased arbor complexity much like that of MADM *trkC*$^{-/-}$ cells (Fig. 1). However, in *math1-Cre;NT-3*$^{flox/flox}$ animals, dendrite defects were rescued to wild-type levels. (**D**) Quantification of height deficiency index. *$P < 0.05$, one-way ANOVA with Tukey's multiple comparisons test. (**E**) Quantification of tdT and GFP/TrkC^{DN} dendritic branch number (top) and cumulative length (bottom). Boxes indicate the mean (middle line) and 25 to 75% range, while whiskers indicate maximum and minimum values. ***$P < 0.001$, two-way ANOVA with Sidak's multiple comparisons test. Also see table S1.

(fig. S1D). Such individually labeled $trkC^{KD/-}$ Purkinje cells exhibited normal dendrite height, branching, and length (Fig. 3, C and D). Thus, in contrast to sparse MADM-based knockout of TrkC, TrkC ablation from all Purkinje cells did not disrupt dendritic arborization.

Differences in the timing of *trkC* removal are unlikely to account for the distinct outcomes of global and sparse knockout (Figs. 1 to 3). *pcp2-Cre* mediated recombination in nearly all Purkinje cells by P7 and markedly reduced *trkC* mRNA levels in Purkinje cells by P10 (fig. S7), well before dendrite phenotypes emerge at P14. A more likely interpretation is that the observed dendrite defects depend on the sparseness of *trkC* deletion. This raised the possibility of a competitive mechanism (*20*), in which dendrite morphogenesis depends on relative differences in TrkC signaling between neighboring Purkinje cells.

We next investigated the expression pattern of NT-3, the ligand for TrkC (*16*), using a *lacZ* knock-in reporter in the *NT-3* locus (*21*). The *lacZ* product β-galactosidase (β-Gal) was transiently expressed at P7 (but not at P14) in a small subset of inferior olive neurons, which extend climbing fibers to Purkinje cell dendrites (Fig. 4A, left). β-Gal was also expressed in cerebellar granule cells, which send parallel fibers to provide major inputs to Purkinje cell dendrites, but was undetectable in the external granular layer, which contains granule cell progenitors (Fig. 4A, middle and right). This suggests that postmitotic granule cells express NT-3 after migrating to the internal granular layer. Although restricted to granule cells in posterior folia at P7 (Fig. 4A, middle), β-Gal was expressed in all folia by P10 (Fig. 4A, right), coinciding with the time window of TrkC-dependent dendritic development (Fig. 1, C and D). Purkinje cell dendrite morphogenesis likely relies on NT-3 produced around or after P10, as dendrite phenotypes of sparse $trkC^{-/-}$ Purkinje cells were equally severe in anterior and posterior folia (fig. S8). Given that β-Gal was undetectable in the deep cerebellar nuclei, the postsynaptic targets of Purkinje cells (Fig. 4A), presynaptic granule cells are the best candidate cellular source of NT-3.

Conditional knockout of NT-3 from granule cell progenitors using *math1-Cre* (*22*) did not affect Purkinje cell dendrite height (fig. S9), branch number, or total length (Fig. 4, B to E). This is consistent with the absence of dendrite phenotypes in Purkinje cell–specific *trkC* knockout (Fig. 3). We next devised a method to investigate NT-3/TrkC signaling in a competitive context (Fig. 4B). Adeno-associated virus serotype 8 (AAV8) preferentially transduces Purkinje cells when injected into neonatal mice (*23*). We exploited this tropism to cotransduce two AAV vectors, the first expressing tdTomato as a control, and the second expressing a dominant-negative TrkC construct (fig. S10) together with GFP ($TrkC^{DN}$-2A-GFP). We achieved sparse labeling (~0.5%) by controlling the titer and volume of neonatal injections (fig. S11). In P21 mice, $TrkC^{DN}$-expressing GFP-positive Purkinje cells exhibited reduced dendrite height, branch number, and total length relative to control, tdTomato-expressing Purkinje cells (Fig. 4, C to E, left columns). This viral approach thus corroborated results from MADM-based sparse knockout.

To test sparse TrkC loss-of-function in the absence of NT-3, we neonatally transduced AAV viruses into conditional knockout mice in which *math1-Cre* removes NT-3 from all granule cells (Fig. 4B). In heterozygous ($NT\text{-}3^{flox/+}$) conditional knockout animals, $TrkC^{DN}$-expressing GFP-positive Purkinje cells still exhibited reduced branching number and length compared to tdTomato-positive control cells (Fig. 4, C to E, middle columns). However, in homozygous ($NT\text{-}3^{flox/flox}$) conditional knockout animals, the dendrite phenotypes of $TrkC^{DN}$-expressing cells were completely suppressed (Fig. 4, C to E, right columns). Thus, granule cell–derived NT-3 is necessary for TrkC-dependent competitive dendrite morphogenesis in Purkinje cells.

In summary, although Purkinje cell dendrite development can proceed in the absence of NT-3 or TrkC, our data indicate that relative intercellular differences in NT-3/TrkC signaling can profoundly modulate dendrite morphogenesis. Specifically, Purkinje cells with lower TrkC levels relative to their neighbors exhibit reduced dendritic arbor complexity. Future studies should elucidate how Purkinje cells compare TrkC levels, and how such intercellular comparisons contribute to normal circuit function. For example, heterogeneous TrkC activation during development may diversify Purkinje cell dendrite complexity, or homeostatically adjust dendrite branching rates to ultimately equalize Purkinje cell participation in the cerebellar circuit. Furthermore, NT-3/TrkC may cooperate with other signals to regulate dendrite development. Although p75NTR likely acts as a receptor for paracrine signals during competitive axon stabilization and pruning (*24*, *25*), we found that sparse *trkC* knockout phenotypes persisted in $p75^{-/-}$ mice (fig. S12), suggesting alternative mechanisms. Indeed, TrkC/NT-3 signaling may mediate competition by enhancing neuronal activity or synaptogenesis, both of which are known to modulate dendritic arborization (*26*, *27*). In one scenario, differential TrkC/NT-3 signaling may drive competitive parallel fiber synapse formation and locally stabilize Purkinje cell dendritic branches. Consistent with this idea, each parallel fiber forms synapses with only a subset of Purkinje cells along its trajectory (*28*), whereas TrkC can mediate postsynaptic differentiation (*17*) and NT-3 can be anterogradely transported and released from central neuron presynaptic terminals (*29*).

According to the classic neurotrophic theory, developing axons compete for limiting amounts of neurotrophic factors from their target tissues, which signal retrogradely to support neuronal survival and axon growth (*30*, *31*). Our findings expand this paradigm and suggest that growing dendrites analogously require anterograde NT-3 from their presynaptic partners during competitive dendrite growth.

REFERENCES AND NOTES

1. E. J. Huang, L. F. Reichardt, *Annu. Rev. Neurosci.* **24**, 677–736 (2001).
2. H. Park, M. M. Poo, *Nat. Rev. Neurosci.* **14**, 7–23 (2013).
3. V. Nikoletopoulou *et al.*, *Nature* **467**, 59–63 (2010).
4. P. C. Maisonpierre *et al.*, *Neuron* **5**, 501–509 (1990).
5. L. Tessarollo *et al.*, *Development* **118**, 463–475 (1993).
6. L. Minichiello, R. Klein, *Genes Dev.* **10**, 2849–2858 (1996).
7. I. Silos-Santiago, A. M. Fagan, M. Garber, B. Fritzsch, M. Barbacid, *Eur. J. Neurosci.* **9**, 2045–2056 (1997).
8. A. K. McAllister, D. C. Lo, L. C. Katz, *Neuron* **15**, 791–803 (1995).
9. A. K. McAllister, L. C. Katz, D. C. Lo, *Neuron* **18**, 767–778 (1997).
10. T. D. Patel *et al.*, *Neuron* **38**, 403–416 (2003).
11. P. Ernfors, K. F. Lee, J. Kucera, R. Jaenisch, *Cell* **77**, 503–512 (1994).
12. H. Zong, J. S. Espinosa, H. H. Su, M. D. Muzumdar, L. Luo, *Cell* **121**, 479–492 (2005).
13. S. Hippenmeyer, R. L. Johnson, L. Luo, *Cell Reports* **3**, 960–967 (2013).
14. L. Tessarollo *et al.*, *Proc. Natl. Acad. Sci. U.S.A.* **94**, 14776–14781 (1997).
15. P. H. Petersen, K. Zou, J. K. Hwang, Y. N. Jan, W. Zhong, *Nature* **419**, 929–934 (2002).
16. E. J. Huang, L. F. Reichardt, *Annu. Rev. Biochem.* **72**, 609–642 (2003).
17. H. Takahashi *et al.*, *Neuron* **69**, 287–303 (2011).
18. X. Chen *et al.*, *Neuron* **46**, 13–21 (2005).
19. X. M. Zhang *et al.*, *Genesis* **40**, 45–51 (2004).
20. C. N. English, A. J. Vigers, K. R. Jones, *Proc. Natl. Acad. Sci. U.S.A.* **109**, 19456–19461 (2012).
21. I. Fariñas, K. R. Jones, C. Backus, X. Y. Wang, L. F. Reichardt, *Nature* **369**, 658–661 (1994).
22. V. Matei *et al.*, *Dev. Dyn.* **234**, 633–650 (2005).
23. D. A. Gibson *et al.*, *Neuron* **81**, 1040–1056 (2014).
24. L. Cao *et al.*, *Curr. Biol.* **17**, 911–921 (2007).
25. K. K. Singh *et al.*, *Nat. Neurosci.* **11**, 649–658 (2008).
26. C. M. Niell, M. P. Meyer, S. J. Smith, *Nat. Neurosci.* **7**, 254–260 (2004).
27. H. Cline, K. Haas, *J. Physiol.* **586**, 1509–1517 (2008).
28. L. Li *et al.*, *PLOS ONE* **5**, e11503 (2010).
29. C. A. Altar, P. S. DiStefano, *Trends Neurosci.* **21**, 433–437 (1998).
30. R. Levi-Montalcini, *Science* **237**, 1154–1162 (1987).
31. L. S. Zweifel, R. Kuruvilla, D. D. Ginty, *Nat. Rev. Neurosci.* **6**, 615–625 (2005).

ACKNOWLEDGMENTS

We thank D. Ginty, L. Tessarollo, and D. Rowitch for mouse lines; the Stanford Gene Vector and Virus Core for AAV production; P. Mehlen and S. Tauszig-Delamasure for advice on cell culture experiments; B. Weissbourd for assistance with in situ hybridization; and T. Clandinin and members of the Luo Lab for helpful discussions and comments on the manuscript. W.J. was supported by the Stanford Neurosciences Graduate Program, the Lorraine Kendall Predoctoral Fellowship Fund, and an NIH National Research Service Award Predoctoral Fellowship (5 F31 NS071697). This research was also supported by an NIH grant (R01-NS050835). L.L. is an investigator of the Howard Hughes Medical Institute. The supplementary materials contain additional data. Stanford University holds a patent on the MADM technology (U.S. Patent 7,282,621) that is described in this paper. The MADM mice are available at the Jackson Laboratory. There is no restriction on sharing all materials with nonprofit organizations. Commercial use of the mice requires a license from Stanford. Please contact Kirsten Leute at kirsten.leute@stanford.edu for more information.

SUPPLEMENTARY MATERIALS

www.sciencemag.org/content/346/6209/626/suppl/DC1
Materials and Methods
Figs. S1 to S12
Table S1
References (*32*–*41*)

21 July 2014; accepted 1 October 2014
10.1126/science.1258996

Dendrite morphogenesis depends on relative levels of NT-3/TrkC signaling

William Joo *et al.*

Science **346**, 626 (2014);
DOI: 10.1126/science.1258996